A numerical study of orbit correction for an asymmetrical motorised momentum exchange tether

Matthew P. Cartmell[1] and Jenna L. Downie[2]
University of Strathclyde, James Weir Building, 75 Montrose Street, Glasgow, G1 1XJ, Scotland, UK

A Motorised Momentum Exchange Tether (MMET) comprises a pair of long lines, ideally in the form of slender tubular structures containing considerable redundancy which connect two orbiting payload masses to a centrally located motor unit. MMETs are intended to be used for orbital payload transportation by which the central motor spins the tether system, against a suitable stator inertia, so that the outer payloads gain suitable velocity to escape orbit in LEO when released. Symmetry is highly desirable as it allows two-way payload flow logistics and it also prevents de-orbit of the tether and the central facility upon payload release. Any scenario in which unexpected payload mass loss occurs, and then initiates asymmetry in the tether, will be potentially catastrophic, and so finding ways to correct the system in this situation is very important. This paper further investigates the dynamics of asymmetrical space tethers to prove that the potential for rescue is possible should such an occurrence arise. The derivation of the equations of motion for an asymmetrical tether is discussed in order to study a tether system with payload unbalance. Partial and full payload losses have been considered, building strongly on previous work, and an analysis of the angular displacement, axial translation, and inertia force acting on the tether has been performed. Centre of mass correction has been proven to be possible through the analysis of partial mass loss; and the centre of mass is shown to be able to correct itself completely, for pragmatic levels of axial correction thrust, given enough time – demonstrating that mission rescue from undesirable asymmetry is possible under the right circumstances.

I. Nomenclature

A	=	solid single tether line cross-sectional area
l	=	tether sub-span length, symmetrical tether
l_1, l_2	=	tether sub-span lengths, asymmetrical tether
M_m	=	facility and motor mass
M_p	=	payload mass, symmetrical tether
M_{p1}, M_{p2}	=	payload masses, asymmetrical tether
n	=	number of discrete mass elements per tether sub-span
r_c, R	=	magnitude of position vector from centre of Earth to centre of mass of the tether system
$r_{facility.}$	=	radius of central facility
$r_{payload}$	=	radius of payload
r_{tether}	=	radius of solid single line tether
r_1	=	magnitude of position vector from centre of Earth to payload 1
r_m, R_m	=	magnitude of position vector from centre of Earth to facility
T_k	=	system kinetic energy
U_p	=	system potential energy

[1] Professor of Nonlinear Dynamics, Department of Mechanical & Aerospace Engineering, Senior Member.
[2] Student, Department of Mechanical & Aerospace Engineering.

This is a peer-reviewed, accepted author manuscript of the following paper: Downie, J. L., & Cartmell, M. P. (2021). A numerical study of orbit correction for an asymmetrical motorised momentum exchange tether. Paper presented at AIAA - ASCEND, United States.

z	=	axial offset coordinate under conditions of tether asymmetry
θ	=	true anomaly
μ	=	standard Newtonian gravitational parameter, equal to GM_E (where M_E is the mass of the Earth)
ρ	=	tether material density
ψ	=	tether spin angle

II. Introduction

The Motorised Momentum Exchange Tether (MMET) was first proposed by Cartmell in 1996 with publication in the open literature in 1998 [1], and in its normal form comprises a pair of identical tether lines connected symmetrically to a motor-driven rotating gantry and with a payload at each end. The two payloads should be of almost identical geometry and mass distribution, but as one is potentially an in-going payload whereas the other is out-going, in terms of the mission architecture, then their physical contents may be very different. The proviso is that they are packed in such a way that the mass distribution within each payload is as close to identical as possible. This requirement allows a form of symmetry to be maintained within the system, essential for proper operation. The rotating gantry is driven by the rotor of a solar powered electric motor and the stator of the motor is connected to two similar tether sub-spans for reaction, in order to satisfy Newton's third law whilst operating on orbit. These tether sub-spans are termed outrigger tethers and in this study are assumed to be deployed so that the propulsion side can operate as intended. Mission architectures for two-way interplanetary operation have been outlined [2] and it has been shown that in principle a motorised tether has the potential to operate continuously in LEO, releasing one payload which has been brought up from Earth by a sub-orbital delivery vehicle into an interplanetary transfer orbit, whilst receiving another from a similar return transfer ready for delivery back down to Earth, as shown in the impression given in Fig. 1. The cylindrical units are the two payloads undergoing propulsion and the spherical units are dummy masses fitted at the ends of the two outrigger tether sub-spans, noting that the length to mass ratios of the outriggers can be scaled to provide correct reaction moments to enable the propulsion side to operate properly. This is not by any means the only application scenario for a MMET but is one that could be of practical use in the future as a sustainable and energy-efficient means of transporting payload mass between the Earth and Moon or the Earth and Mars. Since the MMET is intended to be powered by solar electricity [3] it is an environmentally clean and sustainable system for mass exchange.

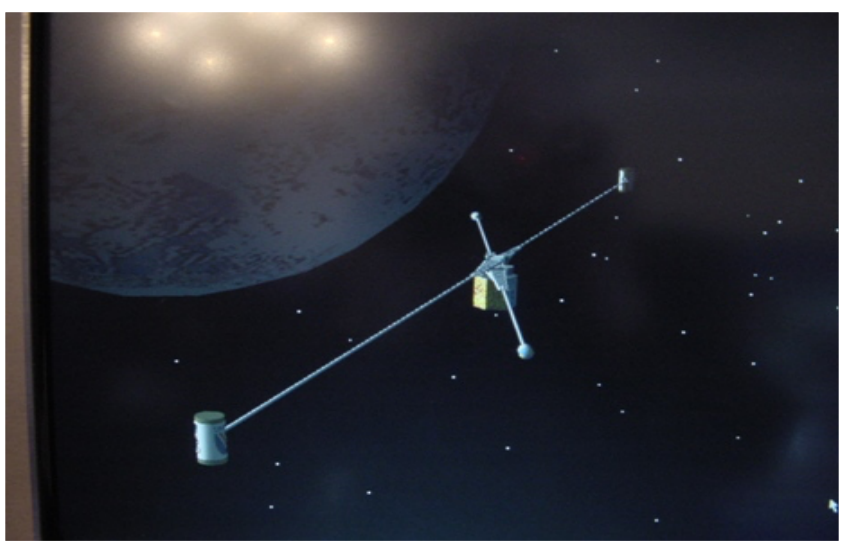

Fig. 1 Conceptual Motorised Momentum Exchange Tether operating in LEO.

The principle of symmetrical operation requires payload release to be exactly simultaneous, with no time delay at all between releases, otherwise the centre of mass of the remaining sub-systems will move. These sub-systems comprise the central facility, the outrigger sub-spans, and the detached propulsion tether sub-spans. Operational asymmetry would have serious repercussions for system retrieval and subsequent continuation of the mission. This is of particular importance for a long-term mission scenario in which the tether is to be re-used over a long time-period, needing precise location and orientation at all times.

It has already been shown [4] that geometrical, and hence mass asymmetry causes an immediately large displacement of the centre of mass of the tether system from the central axis of rotation of the motor-drive within the central facility, to some point far outside the periphery of the central facility. Although this situation is generally retrievable, as shown in [4], the specific de-orbit circumstances for the tether have to be taken closely into account, and that is the principal subject of this paper. It is shown here that different orbits and release asymmetries have different repercussions for the remaining tether components and subsequent recovery scenarios.

III. Mathematical Model of the Tether on Orbit

The planar tether system on orbit about Earth is shown in orbital plan view in Fig. 2(a) and it can be seen there that the natural symmetry of the tether enables a simple dumb-bell system on orbit, as considered in previous publications [1-9], and more widely still. The Earth-fixed frame, *EXY*, provides the overall reference for the problem and the unlabeled position vector from the centre of the Earth, *E*, to the mass centre of the tether, which is geometrically co-located with the central facility at *C*, points to the origin of a local rotating frame of reference, ox_0y_0, and the tether is seen to rotate about the origin of this frame through angle ψ. The sub-spans of the propulsion tethers are identical and each of length l. The payloads are also identical and both of mass M_p. This tidy scenario is disrupted in the geometry of Fig. 2(b), where the instantaneously lower payload, M_{p2} has, for some reason, become detached and has left the system and is shown freely moving to the lower right of the Figure. The post-release geometry is significantly different from that of the symmetrical case just summarised, and so the previous position vector now has to be considered differently. We see in Fig. 2(b) that there are now two significant position vectors to define, firstly r_m which points to the central facility, and secondly r_c which points to the centre of mass location of the system, noting that the system no longer contains payload mass M_{p2}. We also note the position vector to the remaining payload mass M_{p1} and this is denoted by r_1. It is also important to see that the displacement axially along the (instantaneously) lower sub-span l_2 is defined by z and, as first shown in [4], this can be a substantial distance of many km. The aim of any correction that we now apply is to reduce this distance back to zero so that the tether is effectively reset on orbit, even though it is still asymmetrically laden, so that it can then be re-balanced and continue with the mission, notwithstanding the likely need for further reset correction after the re-balancing payload has been attached. Reset is defined by a return to the co-location of *C* with the central facility M_m.

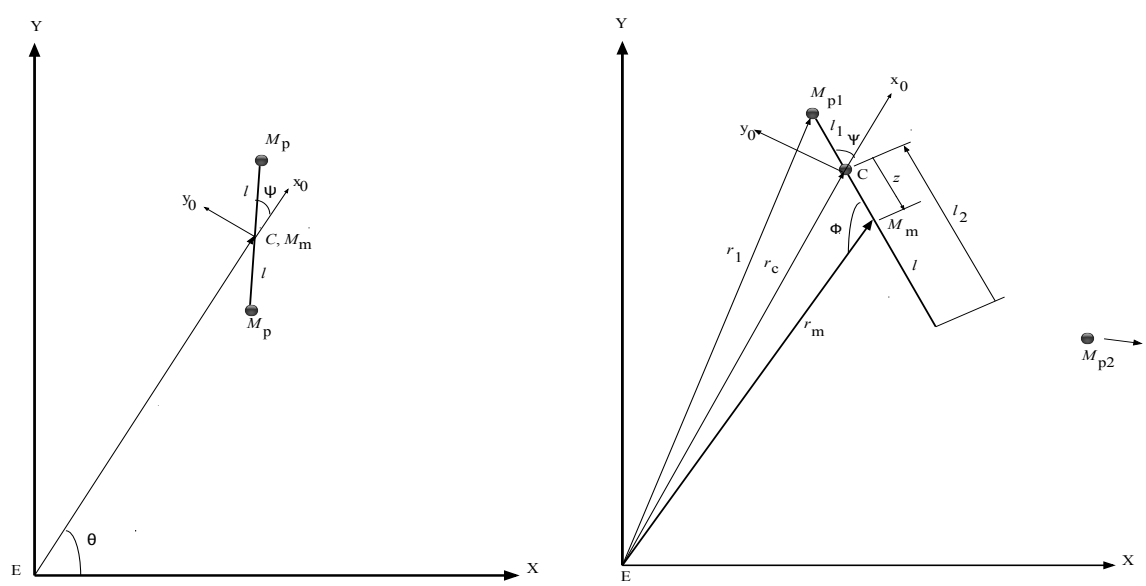

Fig. 2 (a) Planar MMET on orbit in LEO, (b) Immediate post-release configuration for single payload.

The particular instant shown in Fig. 2 (b) confirms that the shorter sub-span l_1 is momentarily uppermost in the diagram when looking down on the orbital plane, and that the longer sub-span l_2 is shown lower down, but as the tether rotates on orbit this varies periodically, with the tether spinning about an axis through the new centre of mass position *C*. In this situation the central facility M_m rotates in a circle of radius z about the new centre of mass position *C*. The free end of the tether which was previously connected mechanically to payload M_{p2} now simply terminates in the

payload shackle fixture (not shown at this level of detail). There would undoubtedly be enough mass within the tether itself, and especially in the shackle, to provide suitable centripetal stiffening of sub-span l_2 as required to maintain the necessary idealisation as a rigid body. We use the true anomaly θ and the spin angle ψ as generalised polar coordinates in the Lagrangian sense, so that the Cartesian positions of the principal masses, M_{p1}, M_{p2} and M_m, which can be determined directly from Fig. 2 (a), can be suitably transformed into polar forms. This can also extend to discretisations of the tether mass in both sub-spans; see Refs. [5-9] for various different investigations using this approach. For a tether system on a circular LEO the simplest representation requires a minimum of one generalised coordinate, defined by ψ, and for a system on an elliptical LEO then this increases to three, defined by ψ, θ, and r_c. If we introduce the asymmetry of Fig. 2(b) then a further generalised coordinate enters the analysis, defined by z. The kinetic energy, T_k, for the asymmetrical system, including the discretised tether mass (where $n = 3$) as well as the payload masses M_{p1} and M_{p2} (noting that the latter could be zero as shown in the case of Fig. 2(b)) and the facility M_m, and therefore accommodating the axial displacement coordinate of the tether, z, is defined by,

$$
\begin{aligned}
T_k = {} & 0.5A\rho(l-z)\Big((r_c\theta'\cos(\theta) + \tfrac{1}{2}(l-z)(\theta'+\psi')\cos(\theta+\psi) - \tfrac{1}{2}z'\sin(\theta+\psi))^2 + (-r_c\theta'\sin(\theta) - \tfrac{1}{2}(l-z)(\theta'+\psi')\sin(\theta+\psi) - \tfrac{1}{2}z'\cos(\theta+\psi))^2\Big) + 0.5A\rho(l+z)\Big((r_c\theta'\cos(\theta) - \tfrac{1}{2}(l+z)(\theta'+\psi')\cos(\theta+\psi) - \\
& \tfrac{1}{2}z'\sin(\theta+\psi))^2 + (-r_c\theta'\sin(\theta) + \tfrac{1}{2}(l+z)(\theta'+\psi')\sin(\theta+\psi) - \tfrac{1}{2}z'\cos(\theta+\psi))^2\Big) + (\theta' + \\
& \psi')^2\big(\tfrac{1}{12}Al\rho(l^2 + 3r_{\text{Tether}}^2) + 0.25r_{\text{facility}}^2 M_m + 0.25M_{\text{p1}}r_{\text{payload}}^2 + 0.25M_{\text{p2}}r_{\text{payload}}^2\big) + 0.5z'^2(2Al\rho + M_m + \\
& M_{\text{p1}} + M_{\text{p2}}) + 0.5M_{\text{p1}}\Big((r_c\theta'\cos(\theta) + (l-z)(\theta'+\psi')\cos(\theta+\psi) + z'(-\sin(\theta+\psi)))^2 + (-r_c\theta'\sin(\theta) - (l- \\
& z)(\theta'+\psi')\sin(\theta+\psi) + z'(-\cos(\theta+\psi)))^2\Big) + 0.5M_{\text{p2}}\Big((r_c\theta'\cos(\theta) + (l-z)(\theta'+\psi')\cos(\theta+\psi) + \\
& z'(-\sin(\theta+\psi)))^2 + (-r_c\theta'\sin(\theta) - (l-z)(\theta'+\psi')\sin(\theta+\psi) + z'(-\cos(\theta+\psi)))^2\Big) + \\
& 0.5M_m\Big((r_c\theta'\cos(\theta) + z'(-\sin(\theta+\psi)) - z(\theta'+\psi')\cos(\theta+\psi))^2 + (-r_c\theta'\sin(\theta) + z'(-\cos(\theta+\psi)) + \\
& z(\theta'+\psi')\sin(\theta+\psi))^2\Big)
\end{aligned}
\tag{1}
$$

The primes denote differentiation with respect to time. Quantities $A, \rho, r_{Tether}, r_{facility}$, and $r_{payload}$ define the cross-sectional area of the tether, the tether material density, the radius of the tether (assuming a single line for the purposes of this investigation, noting that multiple line redundant tethers have been considered in depth in the references), the radius of the central facility and the radius of the two payloads, respectively. The mass moment of inertia of each payload about its own central axis (normal to the spin plane) is $I_{p_{1,2}} = \frac{1}{2}M_{p1,p2}r_{payload}^2$. The mass moment of inertia of the central facility is $I_M = \frac{1}{2}M_m r_{facility}^2$. Also, the mass moment of each of the solid single line tether sub-spans is defined by $I_T = \frac{1}{12}\rho Al(3r_{tether}^2 + l^2)$. These forms have already been substituted into Eq. (1). We can also define the gravitational potential energies for the principal components of the system leading to the following expression for the total system potential energy, U_p,

$$
\begin{aligned}
U_p = {} & -\frac{Al\mu\rho}{3\sqrt{\frac{25l^2}{36} - \frac{5}{3}lR_m\cos(\psi) + {R_m}^2}} - \frac{Al\mu\rho}{3\sqrt{\frac{l^2}{4} - lR_m\cos(\psi) + {R_m}^2}} - \frac{Al\mu\rho}{3\sqrt{\frac{l^2}{36} - \frac{1}{3}lR_m\cos(\psi) + {R_m}^2}} \\
& - \frac{Al\mu\rho}{3\sqrt{\frac{l^2}{36} + \frac{1}{3}lR_m\cos(\psi) + {R_m}^2}} - \frac{Al\mu\rho}{3\sqrt{\frac{l^2}{4} + lR_m\cos(\psi) + {R_m}^2}} - \frac{Al\mu\rho}{3\sqrt{\frac{25l^2}{36} + \frac{5}{3}lR_m\cos(\psi) + {R_m}^2}} \\
& - \frac{\mu M_{\text{p1}}}{\sqrt{l^2 + 2lR_m\cos(\psi) + {R_m}^2}} - \frac{\mu M_{\text{p2}}}{\sqrt{l^2 - 2lR_m\cos(\psi) + {R_m}^2}} - \frac{\mu M_m}{R_m}
\end{aligned}
\tag{2}
$$

The tether mass discretisation scheme of $n = 3$ is adopted for Eq. (2), with three terms per sub-span, one term for each payload and a further term for the central facility, making nine terms in all. Clearly this number of terms increases proportionally with n, and Eq. (2) can be easily re-calculated for any chosen n using a few lines of symbolic computation code written in *Mathematica*™. R_m represents the real-valued r_m shown in Fig. 2(b). Both Eq. (1) & (2) were obtained using symbolic computation to ensure complete correctness. For the case of the motorised tether where the motor drive is designed to provide a torque about the axis through the geometrical centre of the facility and there is no roll of the tether about its own long axis [5], then the generalised force associated with motor drive results in a torque directly driving the differential equation in ψ. This is a special case in the sense that long-axis roll and design

asymmetries cannot be entirely ruled out, but the effects of both could be reduced virtually to zero in practice by means of state-of-the-art orientation control and GNC. Otherwise, we have more complex torque terms which necessitate a further out-of-plane angular coordinate, usually denoted by α, and a further differential equation, and full details of the analysis associated with that approach are given in [5]. For the case under study here, and the simpler circular orbit problem, we are able to reduce the problem down to just two generalised coordinates, ψ and z. In that case we have $\theta = \sqrt{\frac{\mu}{r_c^3}}t$, $\theta' = \sqrt{\frac{\mu}{r_c^3}}$, and $\theta'' = 0$, where the primes denote differentiation with respect to time. Furthermore, analysis of the geometry of the immediate post-release configuration in Fig. 2(b) results in a cubic equation in r_m, [4],

$$r_m(-2lr_c z\cos(\psi) + lr_c^2 + 2r_c z^2\cos(\psi) - r_c^2 z + lz^2 - z^3) - (l - z){r_m}^3 = 0 \tag{3}$$

Physically meaningful roots of this equation, henceforth denoted by R_m, can then be calculated numerically and substituted into Eq. (2) during the remaining stages of symbolic derivation.
However, if we wish to retain more generality and accommodate elliptical orbits then we need four generalised coordinates, ψ, z, θ, and r_c. Eq. (3) provides the means to express this extended system in terms of r_c rather than r_m and clearly the circular orbit constraints given above on θ no longer apply. Irrespective of the orbit required symbolic computation can readily be used to obtain the governing equations of motion by means of classical Lagrangian dynamics, and then these can be solved numerically. The Lagrangian derivation can easily be accommodated by the use of a few appropriate lines of code written in *Mathematica*™, although the length and complexity of these equations precludes us from stating them explicitly here. Symbolic computation provides perfect exactness when obtaining such algebraically complicated differential equations. Numerical solution is then performed within the *Mathematica*™ NDSolve package, using the various controls offered within this package to guarantee convergence and accuracy.

IV. Numerical Results

An in-depth numerical study into the performance of the tether system on different orbits has been undertaken for this paper and a very large amount of data has consequently been generated. Two principal cases are discussed next.

A. Circular Low Earth Orbit

We base this analysis on a consideration of the kinetic and potential energies of the tether over time to uncover the mechanisms behind both circular and elliptical orbit correction. We start with the simplest case of all, when the symmetrical tether is on a circular orbit and the motor drive is off, and so the tether simply aligns with the local gravity vector, defining a 'hanging' tether (for which the necessary initial conditions are simply $\psi(0) = 0$ rad, and $\dot{\psi}(0) = 0$ rad/s). We take a consistent base-line set of data for this discussion, where the sub-span length l is 50km, payload mass M_p is 1000 kg, tether density ρ is 970 kg/m^3, the cross-sectional area A is 62.83 * 10^{-6} m^2, facility mass M_m is 5000 kg, the radii of the facility and the payloads r_m and r_p are both 0.5 m, the length of the position vector from the centre of the Earth to the facility is 6870 km, the gravitation parameter $\mu = GM_E = 3.9877848*10^{14}$ m^3/s^2. For the hanging tether the energies are constant over time, with $T_k \approx 380$ GJ and $U_p \approx$ -760 GJ, so therefore the total energy is $T_k + U_p \approx$ -380 GJ. Clearly these energies are based entirely on constant circular orbital motion and position, respectively, and so the overall system energy remains constant throughout.

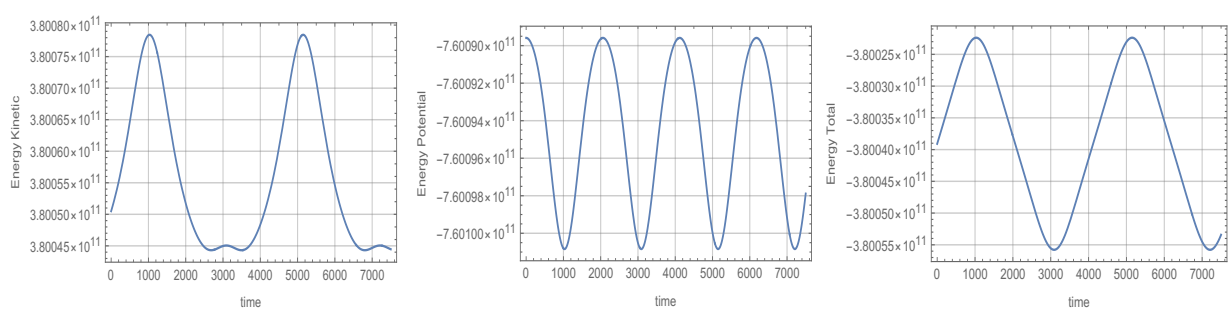

Fig. 3 (a) Kinetic energy (J) over time (s), (b) Potential energy (J) over time (s), (c) Total energy (J) over time (s), for a symmetrical librating unmotorised tether on a circular LEO.

If we now assign a non-zero initial condition to the angular displacement, so $\psi(0) = -0.9$ rad, and $\dot{\psi}(0) = 0$ rad/s, the tether will librate as it travels along the circular orbit. In this case the energies fluctuate periodically, in phase with the libration, and hence with the oscillation of the payload positions with respect to the centre of the Earth, as shown in Fig. 3 (a-c). It's clear from Fig. 3(c) that the total energy of the tether oscillates about a dc offset mean of approximately -380 GJ, corresponding with the constant total energy figure for the hanging tether. Both these cases are for the symmetrical tether. Once we energise the drive motor the scenario changes significantly and the total internal energy of the system necessarily increases over time, as shown in Fig. 4 (a-e) for a torque of $\tau = 25$ MNm. There is no dissipation in this system other than minute amounts of friction within the tether material and construction, which are unmodelled and negligible here, given the very high energy levels typically present in motorised tethers.

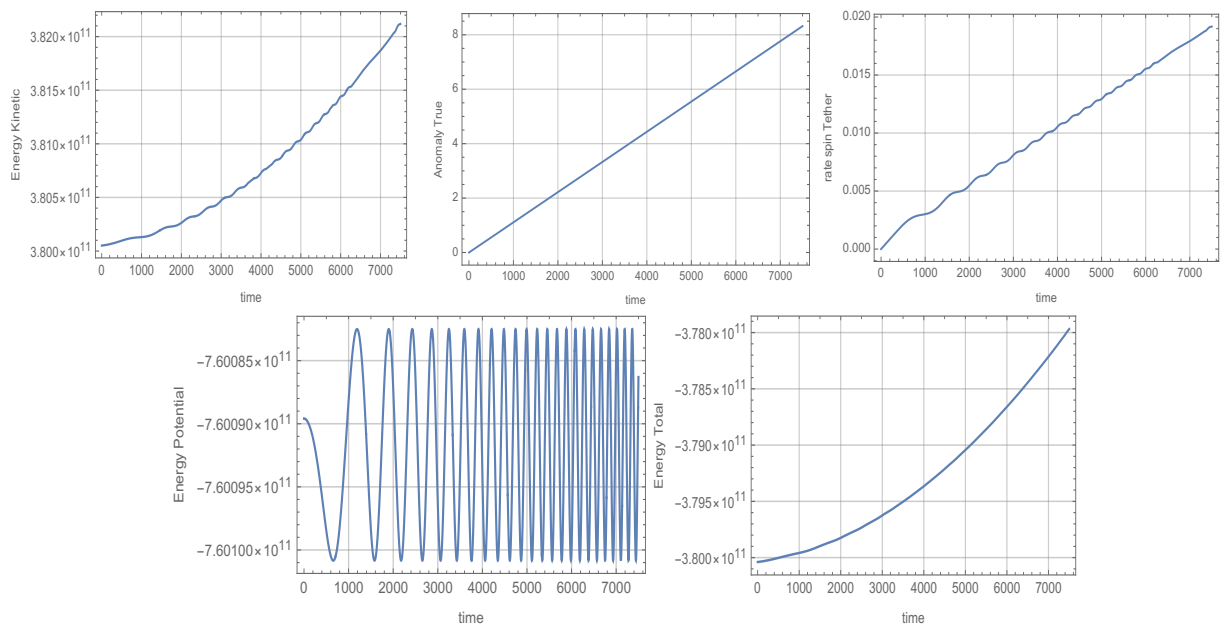

Fig. 4 (a) Kinetic energy (J) over time (s), (b) True anomaly (rad) over time (s), (c) Tether spin rate (rad/s) over time (s), (d) Potential energy (J) over time (s), (e) Total energy (J) over time (s), for a symmetrical spinning motorised tether on a circular LEO.

The spin-rate of the tether shown in Fig. 4(c) increases with the increase in the kinetic energy of the tether, Fig. 4(a), and we also note the linear increase in time of the true anomaly in Fig. 4(b), showing the motion of the whole system on orbit. Because the tether is now spinning monotonically, and accelerating, the potential energy of the tether oscillates over time, and the frequency of the oscillation increases in line with the increasing angular spin-rate of the tether. This is shown very clearly in Fig. 4(d). Fig. 4(e) gives a view of the overall system energy over time, showing how it becomes more positive as the tether spin-rate accelerates. The kinetic effects work against the inherent gravity gradient stabilisation acting on the tether, and have in fact forced it out of the potential well associated with libration.

The next case examines what happens when one of the payloads, arbitrarily chosen to be M_{p2}, suddenly loses 10% of its mass, and this case is summarised in Fig. 5(a-e). This is a milder version of the total payload mass loss case shown diagrammatically in Fig. 2(b), but is important because it qualitatively represents other partial payload mass loss scenarios for circular LEO missions. The tether's position on orbit is corrected, in practice by means of a thruster on payload M_{p2} pulling the whole system along axially, with such an actuation represented here by a constant axial force F_z on the right-hand side of the differential equation in z, and operating during the whole period of payload loss. This force is set to $F_z = 6250$ N, and the tether motor torque is maintained throughout at 25 MNm. We see from Fig. 5(c) that the axial displacement of the tether moves from zero to a maximum of approximately 66 km and then back to zero during the period when the payload has been reduced by 10%, showing a full reset of the tether, such that C and M_m in Fig. 2(b) once again become coincident, over the correction time of approximately 10,000 s. We also note a relatively small modulation of the reset displacement z by the kinetic energy (effectively $\dot{\psi}$), with the modulation depth reaching a maximum at z_{max}. The kinetic energy of the tether starts from a dc offset value of around 380 GJ, see Fig. 5(a), which then oscillates about a mean that increases in line with z. This general characteristic is reflected

in both the potential energy and the total system energy plots as shown in Fig. 5(d) and (e), respectively. It can be seen that the angular spin-rate of the tether is the casualty in this particular scenario and during correction the tether's motion bifurcates back from the monotonic spin to libration, whose peak-to-peak amplitude decreases as the tether approaches z_{max}. In general, we see that the total system energy becomes more positive, up to a maximum at z_{max}, and then drops back to the more negative pre-loss levels as the correction is completed and the tether regains a symmetrical position on orbit, with the necessary internal energy exchange clearly seen between the effect of the work done in axial re-positioning and the libration amplitude.

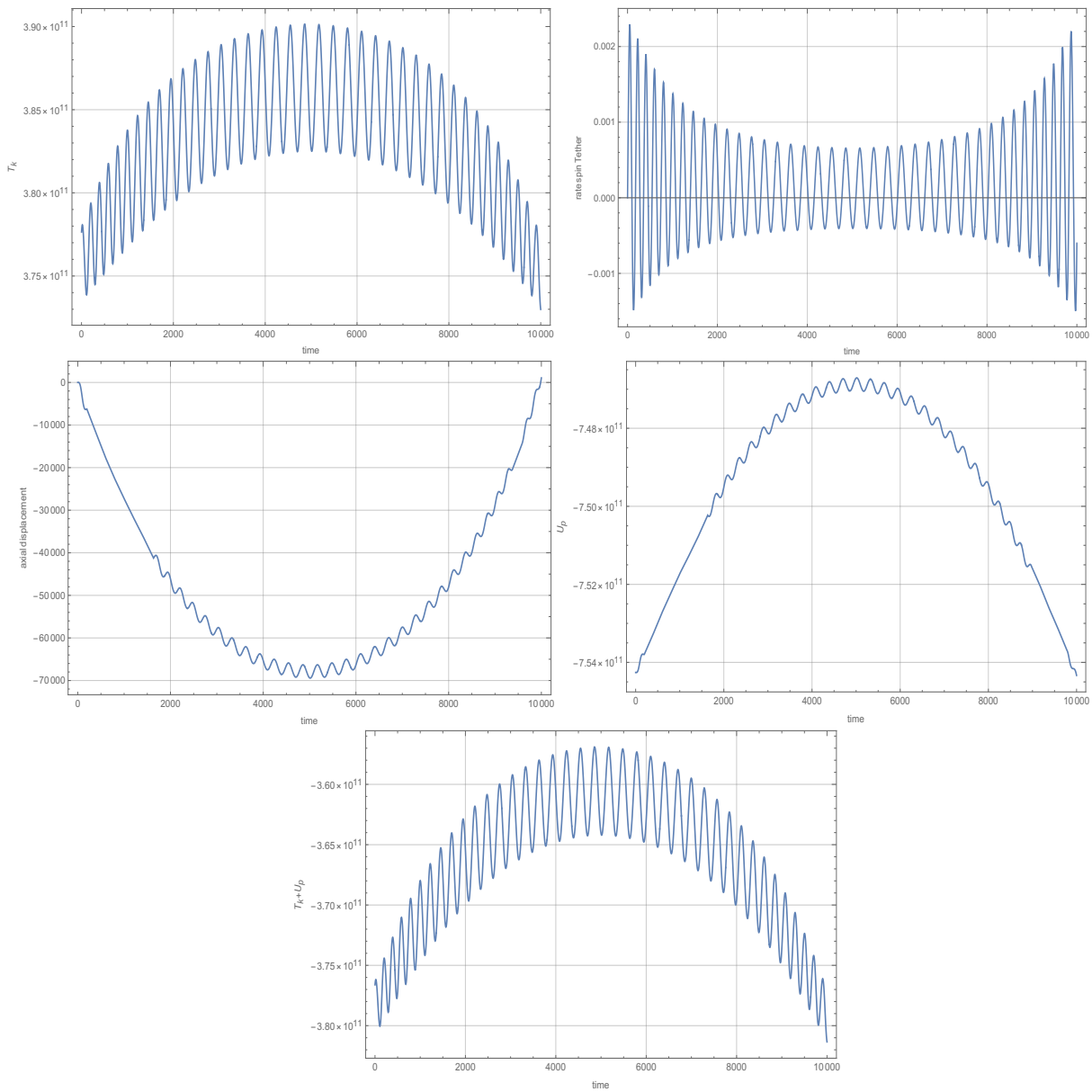

Fig. 5 (a) Kinetic energy (J) over time, (b) Tether spin-rate (rad/s) over time (s), (c) Axial displacement of tether on orbit (m) over time (s), (d) Potential energy (J) over time (s), (e) Total energy (J) over time (s), for an asymmetrical motorised tether on a circular LEO in which payload M_{p2} initially loses 10% of its mass.

We now examine one further case of asymmetry on the circular LEO in which M_{p2} instantaneously loses 90% of its mass, and is therefore set to 100 kg. This case is shown in summary in Fig. 6(a-e), with all other conditions exactly the same as for Fig. 5(a-e), except for a slightly reduced overall integration time, used to scale the graphs optimally.

From Fig. 6(c) we see that in this case the axial displacement of the tether moves from zero to a maximum of about 11 km and then back to zero during the period when the payload has been reduced by 90%, showing that a full reset takes place over the correction time of around 7,300 s. All the phenomena seen in Fig. 5 are qualitatively evident in this case with some quantitative differences to be seen because of the much larger payload loss (and therefore the considerable reduction in overall mass and appropriate mass moments of inertia) for this specific case. Clearly, as the overall mass of the system is greatly reduced on the previous cases there is less inertia to be overcome and therefore the reset time is correspondingly reduced.

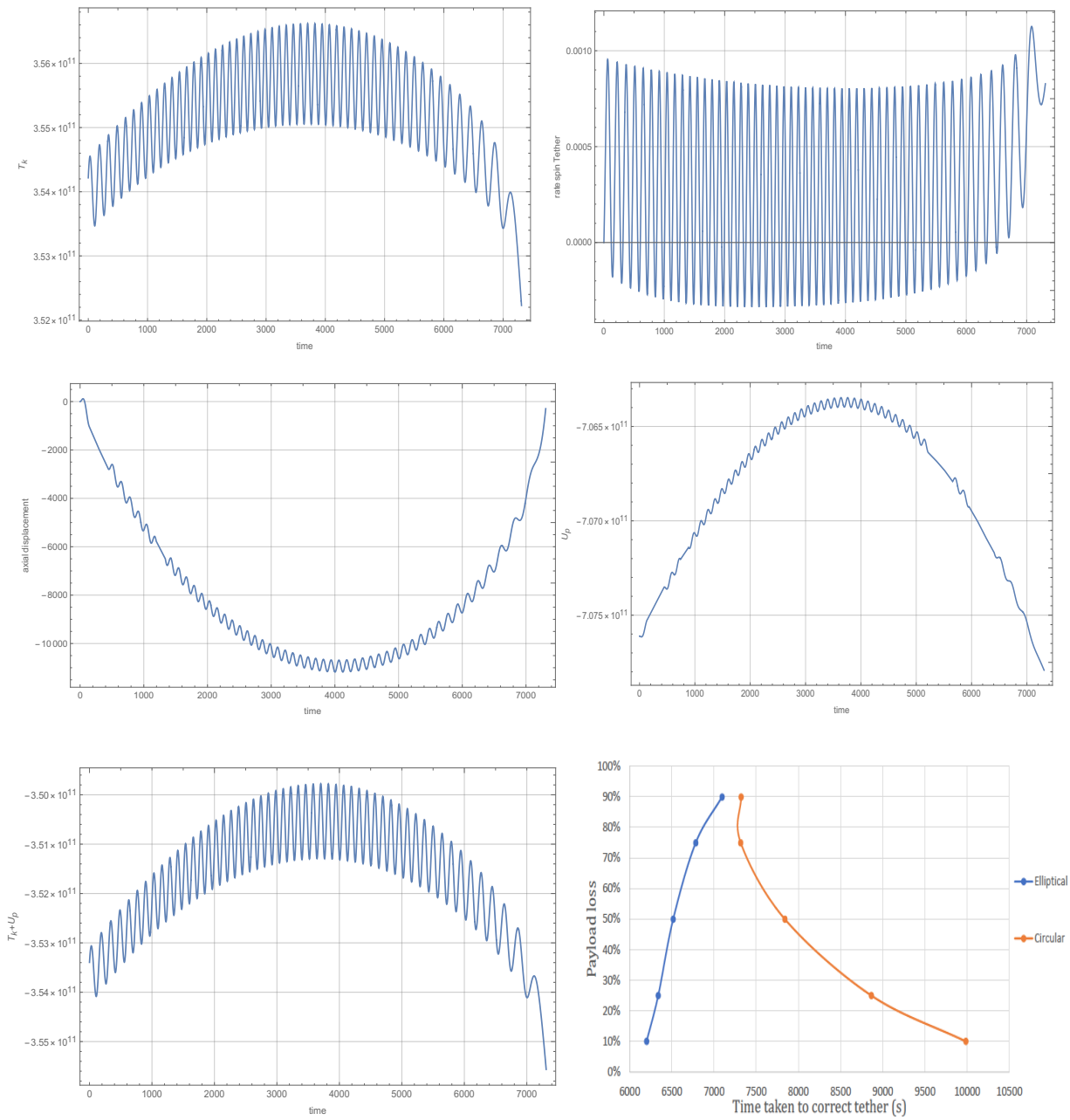

Fig. 6 (a) Kinetic energy (J) over time, (b) Tether spin-rate (rad/s) over time (s), (c) Axial displacement of tether on orbit (m) over time (s), (d) Potential energy (J) over time (s), (e) Total energy (J) over time (s), for an asymmetrical motorised tether on a circular LEO in which payload M_{p2} initially loses 90% of its mass, (f) Payload percentage mass loss as a function of reset time (s), for both circular and elliptical orbits.

The general relationship between reset time and overall system mass is consistent for various circular orbit asymmetry cases in between, and is summarised in Fig. 6(f) (orange line), noting that this Figure also shows the elliptical orbit cases (blue line), to which we refer in section B.

B. Elliptical Low Earth Orbit

Having examined the case of asymmetry when operating on a circular LEO we now look at the case of an elliptical orbit instead, using the same general data as for the circular orbit case. The eccentricity of the orbit examined here is equal to 0.2 based on considerations for practical designs for stable space tethers operating in LEO [5]. The system is now represented by three differential equations in ψ, θ, and R, noting that we use R here to denote orbit radius in place of r_c to avoid confusion with the circular orbit radius. The previous data are all re-used for the motorised symmetrical tether on the elliptical LEO, with the exception of the integration time which is lengthened to 12,000 s in order to accommodate more than one orbit and thereby determine the tether's general performance. The initial conditions are $\psi(0) = 0$ rad, $\dot{\psi}(0) = 0$ rad/s, $R(0) = 6870$ km, $\dot{R}(0) = 0$ m/s, $\theta(0) = 97.1877$ rad, and $\dot{\theta}(0) = 0.00121485$ rad/s. Note that the initial conditions chosen for the orbit radius and true anomaly define the exact perigee of the chosen elliptical orbit, as a convenient maximum-energy point to initialise the tether's subsequent motion. The eccentricity of the orbit is calculated from $e = \frac{R_{apo}-R_{per}}{R_{apo}+R_{per}}$ and the values for the apogee and perigee radii are calculated in a line of *Mathematica*™ code which extracts the numerical maxima and minima from R as it is calculated against time, noting that the apogee radius R_{apo} is the maximal value and the perigee radius R_{per} is the minimal value. The results for this case are shown in Fig. 7(a-f).

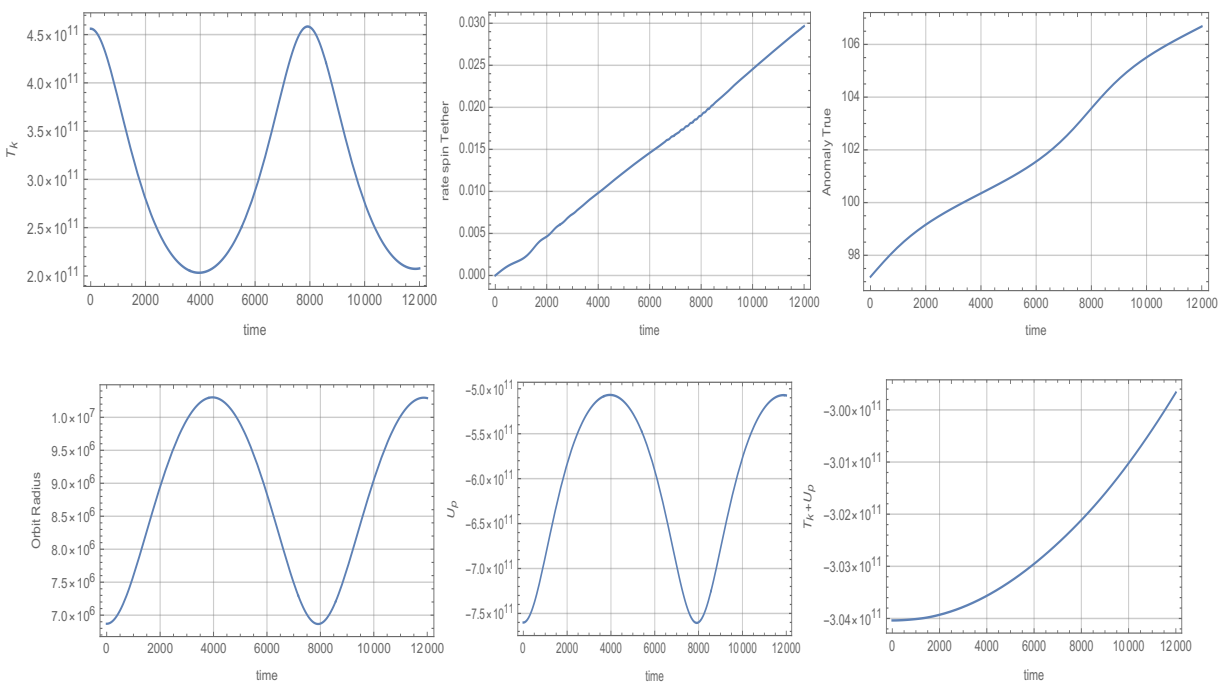

Fig. 7 (a) Kinetic energy (J) over time, (b) Tether spin-rate (rad/s) over time (s), (c) True anomaly (rad) over time (s), (d) Orbit radius (m) over time (s), (e) Potential energy (J) over time (s), (f) Total energy (J) over time (s), for a symmetrical spinning motorised tether on an elliptical LEO, e = 0.2.

We can make direct comparisons between Figs. 4 and 7, as they present the symmetrical tether case for the same data but on circular and elliptical orbits respectively. We see from Fig. 4(f) that the total energy increases positively for the circular orbit, by around 2GJ over around 7,500 s. For the elliptical orbit, in Fig. 7(f), the total energy increases positively by approximately 4GJ over around 12,000 s. So, the rate of energy build up is approximately the same for the two orbits, as one would expect for a tether system that is non-dissipative and excited at the same level on each orbit. The interplay between kinetic and potential energies is where the principal differences lie. In Fig. 4(a) and (d) we see that the kinetic energy builds up monotonically and the potential energy oscillates at a frequency that increases with the angular spin-rate of the tether. In Fig. 7(a) and (e) the situation is different, and the main feature of the kinetic

and potential energies is a low frequency oscillation dependent on the orbit period, but these two energies are phase-shifted in time, and so the total energy, in Fig. 7(f), shows the same sort of monotonic characteristic as it does for the circular orbit. The spin acceleration of the tether is similar for both orbits, and the orbital rate, indicated by the change in the true anomaly over time, is approximately the same in each case. So, the main differences between the two orbits are the qualitative forms of the two energies. We now examine the two asymmetry cases of 10% and 90% payload loss for the elliptical orbit, as summarised in Figs. 8 & 9.

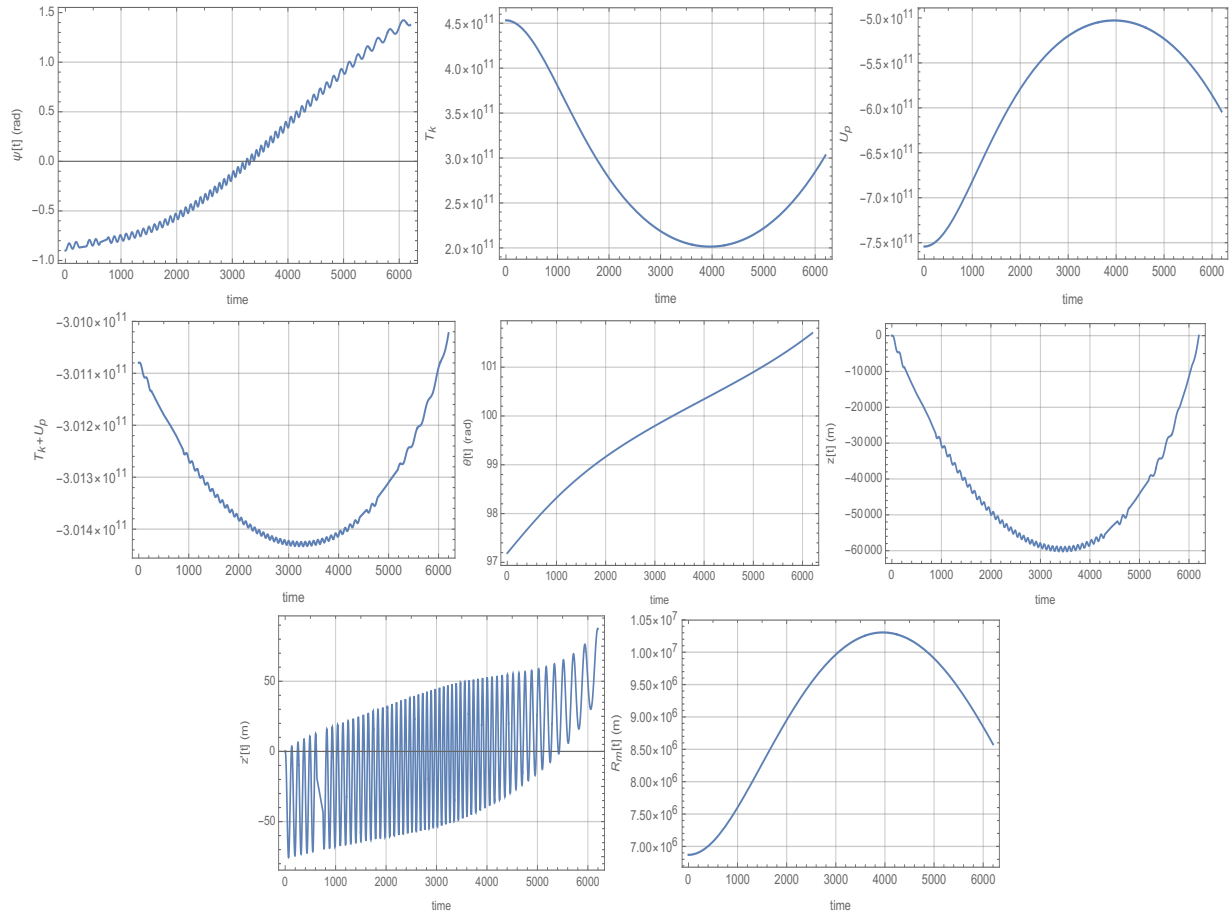

Fig. 8 (a) Tether spin-rate (rad/s) over time (s), (b) Kinetic energy (J) over time (s), (c) Potential energy (J) over time (s), (d) Total energy (J) over time (s), (e) True anomaly (rad) over time (s), (f) Axial displacement of tether on orbit (m) over time (s), (g) Axial velocity of tether on orbit (m) over time (s), (h) Orbit radius (m) over time (s), for an asymmetrical motorised tether on an elliptical LEO, e = 0.2, with 10% payload mass loss.

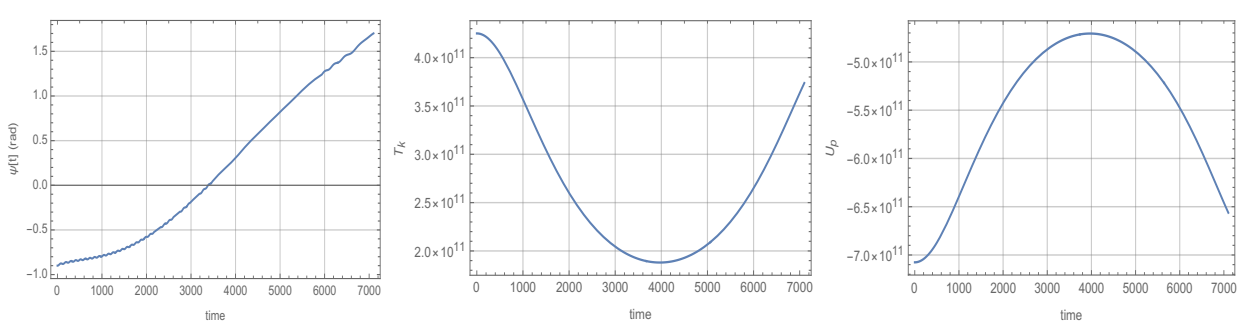

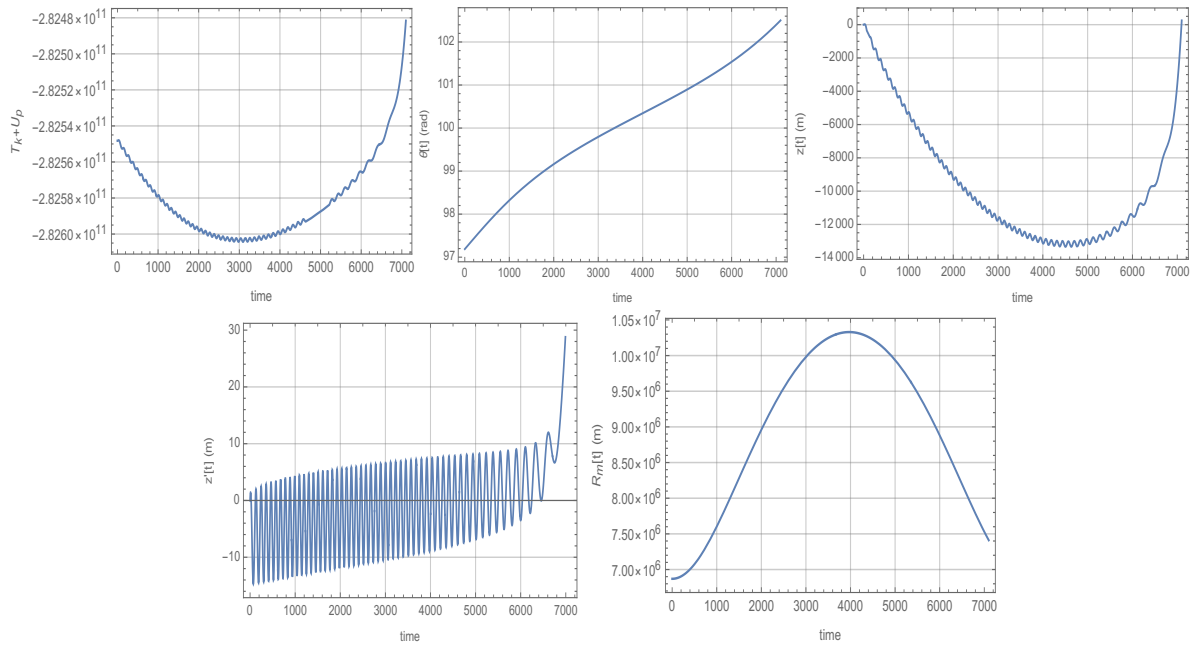

Fig. 9 (a) Tether spin-rate (rad/s) over time (s), (b) Kinetic energy (J) over time (s), (c) Potential energy (J) over time (s), (d) Total energy (J) over time (s), (e) True anomaly (rad) over time (s), (f) Axial displacement of tether on orbit (m) over time (s), (g) Axial velocity of tether on orbit (m) over time (s), (h) Orbit radius (m) over time (s), for an asymmetrical motorised tether on an elliptical LEO, e = 0.2, with 90% payload mass loss.

Examination of Figs. 8(f) and 9(f) in which the axial displacement of the tether z is shown again time, reveals that the system in which there has been a 10% loss in payload mass resets more quickly than the system in which there has been a 90% loss. This is opposite to the circular orbit case (see Figs. 5(c) and 6(c)). In the elliptical orbit case we see that the tether translates through approximately 58 km when 10% of the payload mass is lost, taking approximately 6,200 s, and through approximately 13 km when 90% of the payload mass is lost, taking approximately 7,100 s. The fact that the 'heavier' system (10% payload mass loss) corrects more quickly than the 'lighter' system (90% payload mass loss) seems counter-intuitive but relates directly to the physics of the elliptical orbit and its direct coupling with the local dynamics of the tether. We can get some insight into this by examining the approximate energy levels within the system under these two different payload loss conditions. If we start with the potential energy for the 10% payload loss first, we can see that it ranges from approximately - 510 GJ to – 760 GJ, which we can define as $\left|U_p\right|_{10\%} \approx 250$ GJ. The kinetic energy for this case ranges from approximately 200 GJ to 450 GJ, which we define as $|T_k|_{10\%} \approx 250$ GJ. If we then look at the 90% payload mass loss case then the potential energy is seen to go from approximately – 470 GJ to – 710 GJ, which is defined as $\left|U_p\right|_{90\%} \approx 240$ GJ, and the kinetic energy goes from approximately 185 GJ to 425 GJ, such that $|T_k|_{90\%} \approx 240$ GJ. We see from this that the two energies are equal in each system, and exchange periodically, and also that the energies associated with the heavier system tend to be around 10 GJ higher than those for the lighter system. In fact, a slightly more accurate picture emerges from taking the total energies for the two cases, where we see the that for the 10% payload mass loss case the total system energy varies slightly around a nominal figure of approximately – 301 GJ, whereas the total energy for the 90% payload mass loss case varies slightly around a nominal figure of approximately – 282 GJ, showing a difference in the magnitude of the order of 13 GJ. The 'heavier' system is therefore significantly more energetic on this particular orbit.

Also, for the 10% payload mass loss case the correction force is switched on at t_0, where the initial conditions define the exact perigee of the orbit, and z reaches its maximum excursion at a point just *before* apogee. In the case of the 90% payload mass loss case the correction force is switched on at the same point but we see that z reaches its maximum excursion at a point just *after* apogee. As the orbital velocity is a maximum at perigee and a minimum at apogee, for any elliptical orbit, then we associate perigee with a generally higher kinetic energy, as borne out by Figs. 8(b) and 9(b). So, for the two cases shown here the orbital phasing of the dynamics of the 'heavier' tether and the higher overall energy levels present in that system both together drive the correction to completion within the higher energy portion of the orbit. This is in contrast to the 'lighter' system for which the orbital phasing of the dynamics of the tether and

the lower overall energy levels in that system both together force the correction to complete at a point past apogee and therefore extending into a lower energy portion of the orbit. These findings are also found to be consistent for payload mass losses of 25%, 50%, 75% and 95%, so clearly the effects of phasing of the spin motion of the tether, the axial correction dynamics, and the elliptical orbit all combine to control the timing of the correction, and hence determine the overall characteristic shown by the blue line on Fig. 6(f).

Conclusions

The dynamics of a motorised momentum exchange tether on a circular and elliptical LEO are examined, for cases of symmetrical payload mass distribution and different levels of payload mass asymmetry. The tether is considered here as a planar system, operating solely in the orbital plane, and also as a rigid body due to the inherent effects of gravity gradient stabilisation. We use a reduced order mathematical model in the form of a system of coupled nonlinear ordinary differential equations. The number of generalised coordinates, and hence equations, depends on the complexity of the model. In this paper we go from a symmetrical librating unmotorised planar tether on a simple circular LEO to an asymmetrical spinning motorised planar tether on an elliptical orbit. In all cases the orbital dynamics couple directly to the local dynamics of the tether. We show by analysis that the centre of mass and the centre of the facility are no longer coincident when payload mass asymmetry occurs, and then we show these two points may be brought back to co-location by means of an axial translation of the tether actuated through an additional constant axial force. The results show that in the case of a tether on a circular LEO restoration of this co-location can be achieved more quickly in cases of large payload mass loss, and that the reset time increases nonlinearly with decreasing payload mass loss. The converse is true for the same tether, undergoing the same payload mass asymmetries, when operating on an elliptical LEO, for which $e = 0.2$. This eccentricity is consistent with a small range of orbit eccentricities which encourage stable monotonic spin of the motorised tether, noting that previous work [5] confirmed that extremely complex dynamics can be observed for other regions of eccentricity. For this elliptical orbit it is shown that increasing reset time is nonlinearly proportional to increasing payload mass loss, and that this phenomenon is due to the interplay between the perigee and apogee phasing assuming that the system is initialised at perigee, the degree of asymmetry, and the local dynamics of the tether itself. Higher mass systems (those in which the payload loss is lower) display higher overall energies, interacting with the elliptical orbit in such a manner as to complete the co-location correction reset more quickly during the higher energy portion of the orbit before apogee. Lower mass systems, where the payload mass loss is higher, tend to display lower overall system energies, and the reset takes place over a longer period of the orbit, moving past apogee and into the lower energy portion of the orbit.

Acknowledgment

Jenna L. Downie thanks the Research Interns at Strathclyde programme for the funding made available to her to undertake this research during the summer of 2021.

References

[1] Cartmell, M.P., "Generating velocity increments by means of a spinning motorised tether", *Proceedings of the 34th AIAA/ASME/SAE/ASEE Joint Propulsion Conference and Exhibit*, AIAA, 11 p. A-98-3739.

[2] Cartmell, M.P. & Ziegler, S.W., "Symmetrically laden motorised tethers for continuous two-way interplanetary payload exchange", *Proceedings of the 35th AIAA/ASME/SAE/ASEE Joint Propulsion Conference and Exhibit*, AIAA, 11 p. A-99-2840.

[3] Dalgleish, L.A.F., "A discussion of the physical practicalities of a motorised momentum exchange tether for inter-orbital transfer", ME520 Advanced Research Module Final Report, Department of Mechanical & Aerospace Engineering, University of Strathclyde, Glasgow, UK, 2018.

[4] Cartmell, M.P., Ganilova, O.A., Lennon, E., and Shuttleworth, G., "Motorised momentum exchange space tethers: the dynamics of asymmetrical tethers and some recent new applications", Matec Web of Conferences 2261-336X, Vol 148, 2017, Sofia, Bulgaria, https://doi.org/10.1051/matecconf/201814801001.

[5] Ziegler, S.W., "The rigid body dynamics of tethers in space", PhD thesis, University of Glasgow, Glasgow, UK, 2003.

[6] McKenzie, D.J., "The dynamics of tethers and space-webs", PhD thesis, University of Glasgow, Glasgow, UK, 2010.

[7] Ismail, N.A., "The dynamics of a flexible motorized momentum exchange tether", PhD thesis, University of Glasgow, Glasgow, UK, 2012.

[8] Murray, C., "Continuous Earth-Moon payload exchange using motorised tethers with associated dynamics", PhD thesis, University of Glasgow, Glasgow, UK, 2011.

[9] Cartmell, M.P., & McKenzie, D.J., "A review of space tether research", *Progress in Aerospace Sciences*, Vol. 44, No. 1, 2008, pp. 1-21.